A

Adaptive Calibration for Fusion-based Cyber-Physical Systems

RUI TAN, GUOLIANG XING, Michigan State University, USA
XUE LIU, University of Nebraska-Lincoln, USA
JIANGUO YAO, Shanghai Jiao Tong University, P.R. China
ZHAOHUI YUAN, Wuhan University, P.R. China

Many Cyber-Physical Systems (CPS) are composed of low-cost devices that are deeply integrated with physical environments. As a result, the performance of a CPS system is inevitably undermined by various *physical uncertainties*, which include stochastic noises, hardware biases, unpredictable environment changes and dynamics of the physical process of interest. Traditional solutions to these issues (e.g., device calibration and collaborative signal processing) work in an open-loop fashion and hence often fail to adapt to the uncertainties after system deployment. In this paper, we propose an *adaptive* system-level calibration approach for a class of CPS systems whose primary objective is to detect events or targets of interest. Through collaborative data fusion, our calibration approach features a feedback control loop that exploits system heterogeneity to mitigate the impact of aforementioned uncertainties on the system performance. In contrast to existing heuristic-based solutions, our control-theoretical calibration algorithm can ensure provable system stability and convergence. We also develop a routing algorithm for fusion-based multi-hop CPS systems that is robust to communication unreliability and delay. Our approach is evaluated by both experiments on a testbed of Tmotes as well as extensive simulations based on data traces gathered from a real vehicle detection experiment. The results demonstrate that our calibration algorithm enables a CPS system to maintain the optimal sensing performance in the presence of various system and environmental dynamics.

Categories and Subject Descriptors: B.8.1 [**Performance and Reliability**]: Reliability, Testing, and Fault-Tolerance; C.3 [**Special-purpose and Application-based Systems**]: Signal processing systems

General Terms: Measurement, Performance, Reliability

Additional Key Words and Phrases: Calibration, data fusion, feedback control, Cyber-Physical Systems

ACM Reference Format:
Tan, R., Xing, G., Liu, X., Yao, J., Yuan, Z. 2010. Adaptive calibration for fusion-based cyber-physical systems. ACM Trans. Embedd. Comput. Syst. V, N, Article A (January YYYY), 24 pages.
DOI = 10.1145/0000000.0000000 http://doi.acm.org/10.1145/0000000.0000000

1. INTRODUCTION

Cyber-Physical Systems (CPS) interact with the physical world by tightly integrating sensing, actuation, computation, and communication with physical processes. In recent years, CPS systems are increasingly deployed in mission-critical applications such

The work described in this paper was partially supported by the National Science Foundation under a CAREER grant CNS-0954039, Canadian NSERC Discovery Grant 341823-07, NSERC Strategic Grant STPGP 364910-08, and FQRNT grant 2010-NC-131844.
Authors' addresses: R. Tan and G. Xing, Department of Computer Science and Engineering, Michigan State University, East Lansing, MI 48824-1226, USA; X. Liu, Department of Computer Science and Engineering, University of Nebraska-Lincoln, Lincoln, NE 68588-0150, USA; J. Yao, School of Software, Shanghai Jiao Tong University, Shanghai 200240, P.R. China; Z. Yuan, Wuhan University, Wuhan 430072, P.R. China.

DOI 10.1145/0000000.0000000 http://doi.acm.org/10.1145/0000000.0000000

as security, civil infrastructure, manufacturing, and transportation. In these applications, low-cost sensors and actuators are deeply embedded in physical environments and hence often suffer significant performance variations. In particular, the sensing performance of a CPS system is greatly affected by stochastic noises, hardware biases, unpredictable environment changes and dynamics of the physical process of interest. In order to achieve desirable system performance, the operational parameters of a system must be dynamically calibrated in response to these uncertainties.

Several approaches have been proposed to deal with the aforementioned uncertainties faced by CPS systems. Advanced collaborative signal processing algorithms such as data fusion [Varshney 1996] can mitigate the impact of noise by jointly considering the measurements of multiple sensors. However, these algorithms are not designed to handle hardware biases or environmental dynamics. Sensor calibration [Ramanathan et al. 2006; Feng et al. 2003; Whitehouse and Culler 2002] can correct hardware biases by tuning each individual sensor, which does not exploit the collaboration among sensors in data fusion. Moreover, most existing calibration and data fusion schemes either require expected models of real processes of interest, or need to be trained based on ground truth information of controlled processes [Ramanathan et al. 2006]. Such an offline, open-loop approach is ill-suited for CPS systems because the processes of interest may not match the expectation at the design time or are subject to evolution. For instance, an acoustic sensor system that is trained to detect military vehicles may yield excessive false negatives when the targets of interest are changed to human intruders whose acoustic energy profiles are significantly different from vehicles.

In this paper, we exploit the heterogeneity of CPS systems to achieve adaptive sensing performance. Many practical CPS systems have multiple sensor modalities. For instance, a typical surveillance system [Wren et al. 2006] has both *low-end* passive infrared or acoustic sensors and *high-quality* pan-tilt-zoom cameras. Low-end sensors consume less energy but often have limited sensing capability such as high false alarm rate. In contrast, high-quality sensors can yield high-fidelity measurements at the price of high energy consumption. Moreover, due to the high manufacturing cost, the number of high-end sensors is often small leading to limited sensing coverage. The trade-offs between power consumption and sensing performance of different sensor modalities have been exploited to achieve energy efficiency in sensor networks before [Dutta et al. 2005]. We exploit the heterogeneity in a system by using the results of high-quality sensors to periodically calibrate low-end sensors such that the system sensing performance can adapt to various uncertainties. Specifically, low-end sensors collaboratively sense information of environments through data fusion [Varshney 1996]. When a positive sensing consensus is reached by low-end sensors, high-quality sensors are activated to carry out high-fidelity sensing. The results can accurately capture the spatiotemporal variations of targets of interest. For instance, a camera can easily recognize new targets of interest based on advanced image processing algorithms. The results can in turn be used to calibrate low-end sensors (e.g., acoustic sensors or accelerometers) that are sensitive to the characteristics (e.g., acoustic or seismic energy profile) of targets. Moreover, the high-quality sensors are allowed to sleep for most of the time and only activated when a possible event of interest is sensed by low-end sensors. Such a two-tier calibration framework can significantly reduce system energy consumption while maintaining satisfactory sensing performance in dynamic environments.

Several challenges must be addressed for calibrating the system performance of heterogeneous CPS systems. First, the system sensing performance is tightly coupled with the measurements of low-end sensors that are often corrupted by random noises from physical environment and hardware. The stochastics in sensor measurements must be carefully considered in order to achieve the optimal sensing performance. Second, in

an adaptive calibration process, there exist fundamental trade-offs between the system stability and the delay of response to system and environmental dynamics. Such trade-offs must be balanced to maintain satisfactory system stability and timeliness. Third, the system calibration performance is inherently impacted by the underlying communication network. An adaptive calibration algorithm must account for various dynamic characteristics of wireless communications, such as link reliability, delay, and routing quality.

We make the following major contributions in this paper.

— We propose a novel approach that exploits sensor heterogeneity for adaptively calibrating the performance of fusion-based CPS systems. In our approach, high-quality sensors are activated only when low-end sensors sense a possible event of interest. The sensing results of high-quality sensors are then fed back to low-end sensors for tuning their performance.
— We formally formulate the problem of adaptive calibration for event detection as a control problem. The system objective is to maximize the detection performance and adapt to variable system conditions and physical environments. We develop an adaptive calibration algorithm based on feedback control theory. We also systematically analyze the impacts of several communication issues such as communication reliability and delay, and propose an optimal routing algorithm that minimizes the impact of packet loss on system stability. Moreover, we extend our approach to address various data fusion schemes and rapidly changing dynamics of the monitored physical process.
— We implement the adaptive calibration algorithm on a testbed composed of Tmotes [Moteiv Corp. 2006] and a camera. We also conduct extensive trace-driven simulations using real data traces collected by 17 sensors in a vehicle detection experiment [Duarte and Hu 2004]. The results demonstrate that the calibrated system maintains optimal detection performance in the presence of various system and environmental dynamics.

The rest of this paper is organized as follows. Section 2 reviews related work. Section 3 introduces the preliminaries and Section 4 formally formulates the adaptive calibration problem. Section 5 models the system detection performance of a fusion-based CPS system. Section 6 develops the adaptive calibration algorithm based on control theory. Section 7 discusses the impacts of communication performance. Several extensions are discussed in Section 8. Section 9 and 10 present the experimental results of hardware testbed and trace-driven simulations, respectively. Section 11 concludes this paper.

2. RELATED WORK

Calibration is a fundamental problem in CPS systems. Early work focuses on calibrating individual devices (e.g., sensors and actuators) independently. For instance, in [Ramanathan et al. 2006], each chemical sensor is carefully calibrated in controlled environments to obtain the mapping from its reading to the true value. Recent system-level calibration approaches aim to optimize the overall system performance. In [Feng et al. 2003], the biases of light sensors are estimated by solving the equations that correlate the sensor biases with the sensor measurements. In [Whitehouse and Culler 2002], the operational parameters of ranging sensors are estimated by regression based on pairwise range measurements. In [Kim et al. 2008] and [Kim et al. 2009], the fine-grained water and electrical power usage reports are generated according to the measurements of distributed sensors. The calibration parameters for the sensors are estimated by regression based on the total usage readings from the main water/power meter. Different from the above approaches that calibrate sensors according to known ground truth in-

puts, the *blind* calibration approaches [Bychkovsky et al. 2003; Balzano and Nowak 2007] do not require ground truth inputs. In [Bychkovsky et al. 2003], the discrepancies among co-located sensors are eliminated by exploiting the spatial correlation in their measurements, where the ground truth is unnecessary. However, in order to leverage the correlation among sensors, the blind approaches require the prior knowledge of the signal of interest, e.g., the spatial frequency. Sensor localization is often formulated as a calibration problem [Ihler et al. 2004; Girod et al. 2006]. Sensors estimate their relative positions according to the noisy ranging measurements (e.g., acoustic ranging [Girod et al. 2006]). The relative positions can be translated into absolute positions if a subset of nodes have ground truth GPSs. Different from the above works, we aim to calibrate the operational parameters of a fusion-based CPS system to achieve optimal event detection performance. Moreover, by exploiting sensor heterogeneity, our approach does not require ground truth inputs and only needs some prior knowledge of the target of interest, i.e., the target appearance probability.

Feedback control has been widely adopted to improve the adaptability of computing systems and networks [Adbelzaher et al. 2008]. Recently, it is employed to develop various protocols for CPS and sensor systems, such as MAC-layer [Le et al. 2007], energy management [Vigorito et al. 2007] and topology control [Shi et al. 2007] protocols. Different from these works, we develop a control-theoretical calibration algorithm that maximizes the event detection performance of a CPS system under dynamic system conditions and physical environments. In our recent work [Chen et al. 2010], we developed a feedback control based approach to enforce a system CPU utilization bound while maximizing event detection probability. However, sensor calibration is not addressed in [Chen et al. 2010].

Data fusion [Varshney 1996] has been proposed as an effective signal processing technique to improve the system detection performance of sensing applications [He et al. 2004; Duarte and Hu 2003]. Most previous works [Varshney 1996; Clouqueur et al. 2004] focus on analyzing the optimal fusion strategies of a given sensor system. In our recent work [Xing et al. 2009; Tan et al. 2009], we investigated the impact of data fusion on coverage and detection delay of sensor networks. In this paper, we aim to adaptively calibrate the fusion parameters to increase system sensing performance in the presence of dynamics of environment and monitored physical processes.

3. PRELIMINARIES

In this work, we focus on the CPS systems whose primary objective is to detect events/targets of interest. Traditional surveillance sensor systems are often designed based on offline calibration and work in an open-loop fashion. As a result, they often yield poor detection performance when the physical reality does not match the expectation. A key advantage of our approach is that it enables a CPS system to automatically adapt to the dynamics of environments or monitored physical processes. In this section, we present the preliminaries of our work, which include sensor measurement, data fusion and Bayesian detection models.

3.1. Sensor Measurement Model

We assume that sensors perform detection by measuring the energy of signals, e.g., acoustic signal, emitted by the target. Let s_i denote the signal energy received by sensor i. The signal energy s_i varies with the target and sensor i due to several affecting issues. First, the signal energy s_i depends on the source energy of the target and the signal path loss. The signal path loss is determined by the distance from the target and the physical environments such as terrain. Second, it is affected by the systematic bias of the sensor.

Table I. Summary of Notation

Symbol	Definition
H_0 / H_1	the ground truth that the target is absent / present
$\widetilde{H}_0$ / $\widetilde{H}_1$	cluster head's decision that the target is absent / present
μ_i, σ_i^2	noise mean and variance of sensor i, respectively
s_i	the signal energy received by sensor i
n_i	noise energy of sensor i, $n_i \sim \mathcal{N}(\mu_i, \sigma_i^2)$
y_i	signal energy measurement of sensor i
N	the number of sensors in the cluster concerned
Y	fused measurement, $Y = \sum_{i=1}^{N} y_i$
μ / σ^2 / S	$\mu = \sum_{i=1}^{N} \mu_i$, $\sigma^2 = \sum_{i=1}^{N} \sigma_i^2$, $S = \sum_{i=1}^{N} s_i$
C_{ij}	the cost of deciding $\widetilde{H}_i$ when the ground truth is H_j
m	the number of detections in a calibration cycle
P_{FL} / P_{ML}	false alarm rate / missing probability of low-end sensors
P_{FH} / P_{MH}	false alarm rate / missing probability of high-quality sensor
P_a	target appearance probability, $P_a = \mathbb{P}(H_1)$
D	the lower bound of target appearance time

The sensor measurements are contaminated by additive random noises from sensor hardware or environment. For instance, the electronic noise is a common noise source for sensor circuits. Depending on the hypothesis that the target is absent (H_0) or present (H_1), the measurement of sensor i, denoted by y_i, is given by

$$\begin{cases} H_0: \ y_i = n_i, \\ H_1: \ y_i = s_i + n_i, \end{cases}$$

where n_i is the energy of noise experienced by sensor i. We assume that the noise n_i at each sensor i follows the normal distribution, i.e., $n_i \sim \mathcal{N}(\mu_i, \sigma_i^2)$, where μ_i and σ_i^2 are the mean and variance of n_i, respectively. We assume that the noises, $\{n_i|\forall i\}$, are spatially independent across sensors.

The above stochastic sensor measurement model has been widely adopted in the literature of multi-sensor signal detection [Clouqueur et al. 2004; Li and Hu 2003; Sheng and Hu 2005; Varshney 1996; Xing et al. 2009; Tan et al. 2009] and also empirically verified [Hata 1980; Li and Hu 2003; Tan et al. 2009]. Many previous works [Clouqueur et al. 2004; Li and Hu 2003; Sheng and Hu 2005; Xing et al. 2009; Tan et al. 2009] based on the above sensor measurement model assume that the signal energies $\{s_i|\forall i\}$ and noise profiles $\{\mu_i, \sigma_i^2|\forall i\}$ are known *a priori*. However, these parameters are often difficult to estimate and also subject to change due to the dynamics of target and environment. In this paper, we assume that they are unknown to the system.

Table I summarizes the notation used in this paper.

3.2. Data Fusion and Bayesian Detection Models

Data fusion [Varshney 1996] is an effective signal processing technique to improve the performance of CPS and sensor systems. A CPS system that employs data fusion is often organized into clusters. The cluster head is responsible for making a decision regarding the presence of an event by fusing the information gathered by member sensors. There exist two basic data fusion schemes, namely, *decision fusion* and *value fusion*. In decision fusion, each sensor makes a *local* decision based on its measurements and sends its decision to the cluster head, which makes a *system* decision according to the local decisions. In value fusion, each sensor sends its measurements to the cluster head, which makes the detection decision based on the received measurements. In this

paper, we first focus on value fusion and then extend our approach to a decision fusion model in Section 8.2.

Suppose there are N sensors in a cluster. If the noises experienced by sensors are independent and follow Gaussian distribution, the optimal test statistics for value fusion is $\sum_{i=1}^{N} \frac{s_i}{\sigma_i^2} \cdot y_i$ [Duda et al. 2001]. However, as discussed in Section 3.1, s_i and σ_i are unknown. Therefore, we employ the equal gain combination which has been widely adopted by previous literature on signal detection [Clouqueur et al. 2004; Xing et al. 2009]. Specifically, the test statistics, denote by Y, is given by $Y = \sum_{i=1}^{N} y_i$. The cluster head makes a positive decision (denoted by $\widetilde{H}_1$) if Y exceeds a threshold; otherwise, it makes a negative decision (denoted by $\widetilde{H}_0$). The *system* detection performance is characterized by two metrics, namely, the false alarm rate (denoted by P_F) and missing probability (denoted by P_M). P_F is the probability of deciding $\widetilde{H}_1$ when *no* target is present, and P_M is the probability of deciding $\widetilde{H}_0$ when a target is present. Formally, $P_F = \mathbb{P}(\widetilde{H}_1|H_0)$ and $P_M = \mathbb{P}(\widetilde{H}_0|H_1)$.

The Bayesian criterion is a widely adopted decision criterion for detection systems [Duda et al. 2001; Varshney 1996]. The objective of Bayesian detection is to minimize the expected cost or risk in making decisions, which is denoted by $\mathbb{E}[c]$ and formally given by [Duda et al. 2001]:

$$\mathbb{E}[c] = \sum_{i\in\{0,1\},j\in\{0,1\}} C_{ij} \cdot \mathbb{P}(\widetilde{H}_i|H_j) \cdot \mathbb{P}(H_j), \tag{1}$$

where C_{ij} is the cost of deciding $\widetilde{H}_i$ when the ground truth is H_j and $\mathbb{P}(H_j)$ is the prior probability of the ground truth H_j. Note that the costs, i.e., $\{C_{ij}|i,j \in \{0,1\}\}$, are constants specified by user. In practice, $\{C_{ij}|i,j \in \{0,1\}\}$ can be defined according to various system objectives. For instance, by letting $C_{00} = C_{11} = 0$ and $C_{10} = C_{01} = 1$, $\mathbb{E}[c]$ equals the expected probability that the detector makes wrong decisions over all possible measurements [Duda et al. 2001], i.e., the average error rate. Moreover, by letting C_{ij} be the energy consumed in the operations triggered by deciding $\widetilde{H}_i$ when the ground truth is H_j, $\mathbb{E}[c]$ is the average energy consumed by the system due to detection.

4. PROBLEM FORMULATION

This section formulates our problem. Section 4.1 presents the system and target models. Section 4.2 formally formulates the closed-loop calibration problem. Section 4.3 presents the overview of our approach to the problem.

4.1. System and Target Models

We assume that a heterogeneous CPS system is composed of *low-end* and *high-quality* sensors. The objective is to detect targets that randomly appear. The low-end sensors (e.g., MICA motes) often have low manufacturing cost and energy consumption. However, they usually have limited sensing capability such as high false alarm rate [He et al. 2004]. To improve the system detection performance, the low-end sensors collaboratively detect targets by fusing their measurements as stated in Section 3.2. The high-quality sensors (e.g., cameras [Wren et al. 2006] and active radars [Dutta et al. 2006]) are capable of high-accuracy and complex surveillance such as target tracking and classification. In this paper, they are only required to detect whether a target is present and the detection results are used to calibrate the low-end sensors to achieve desirable detection performance. The high-quality sensors often have higher manufacturing cost and consume more energy. Due to the high cost, we assume that there is

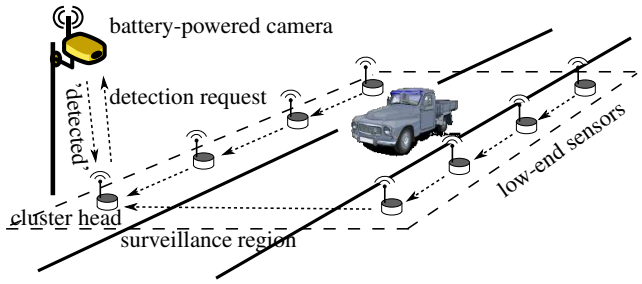

Fig. 1. The illustration of system architecture. The system composed of multiple low-end sensors and a high-quality sensor detects whether a vehicle is present in the rectangular surveillance region.

only one high-quality sensor in the system. We note that our approach can be easily extended to the scenarios of multiple high-quality sensors where they may fuse their measurements to yield more accurate detection results.

We now illustrate the system architecture using an example shown in Fig. 1. Suppose an ad-hoc CPS system is deployed to detect whether a vehicle is present in the surveillance region. The system is composed of a battery-powered camera and a number of low-cost acoustic sensors. The acoustic sensors transmit their measurements to the cluster head through multi-hop paths. The cluster head fuses the received measurements to make a detection decision regarding the presence of the vehicle. The camera can accurately detect the vehicle via image processing techniques. However, the camera often consumes much energy in capturing and processing images. The objective is to calibrate the acoustic sensors according to the detection results of the camera such that the detection performance of the system is maximized. The calibrated system should be able to adapt to the unpredictable and dynamic changes of the target profiles and physical environments. Moreover, in order to save energy, the camera should be allowed to sleep when no vehicle is present in the surveillance region.

Before formally formulating the problem, we make the following assumptions. First, the probability that a target is present at any time instance is P_a which is known or can be estimated from detection history. In Section 8, we will discuss how to address unknown and changeable P_a. Second, the target appearance time is lower-bounded by constant D. Third, the false alarm rate and missing probability of the high-quality sensor, denoted by P_{FH} and P_{MH}, are known. For instance, P_{FH} and P_{MH} can be measured via offline experiments. Due to the high accuracy of the high-quality sensor, both P_{FH} and P_{MH} are close to zero.

4.2. Closed-loop Calibration Problem

The optimal Bayesian detector has been extensively studied in previous literature [Varshney 1996; Duda et al. 2001]. We now investigate the optimal detection rule for low-end sensors under the assumptions made in Section 3. Suppose there are N low-end sensors. Denote $S = \sum_{i=1}^{N} s_i$, $\mu = \sum_{i=1}^{N} \mu_i$ and $\sigma^2 = \sum_{i=1}^{N} \sigma_i^2$. The optimal detection rule for low-end sensors that minimizes the expected cost $\mathbb{E}[c]$ is given by a threshold-based decision (the derivation can be found in Appendix A), i.e., $Y \underset{\widetilde{H}_0}{\overset{\widetilde{H}_1}{\gtrless}} T_{\text{opt}}$, where Y is the sum of the measurements from low-end sensors and the optimal detection thresh-

old T_{opt} is given by

$$T_{\text{opt}} = \frac{\delta\sigma^2}{2S} + \mu + \frac{S}{2}, \tag{2}$$

$$\delta = 2\ln\left(\frac{1-P_a}{P_a} \cdot \frac{C_{10}-C_{00}}{C_{01}-C_{11}}\right). \tag{3}$$

Note that δ is a known constant as long as P_a and $\{C_{ij}|i,j \in \{0,1\}\}$ are given.

In the above optimal detection rule, the optimal detection threshold T_{opt} is often unknown and cannot be easily estimated in practice. First, μ and σ^2 are the sums of noise means and variances at all low-end sensors, respectively. Although the noise means and variances can be estimated offline (e.g., in laboratory), they may change at run time. For instance, the noise profiles would change with environmental conditions (e.g., wind) as well as the electronic noise in sensor hardware affected by ambient temperatures. Second, S is the sum of signals received by low-end sensors and hence is affected by the source energy and physical position of the target. However, both the source energy and position of the target are unknown and changeable in practice. Moreover, if the ground truth information is not available, the detection approaches based on the inaccurate μ, σ^2 and S that are estimated from noisy measurements may lead to poor system detection performance. As a result, implementing the optimal detection rule based on unknown μ, σ^2 and S is largely unpractical.

In this paper, we exploit sensor heterogeneity to address the issue of unknown μ, σ^2 and S. As the high-quality sensor can detect the target accurately, the detection results can be fed back to calibrate the low-end sensors when the target profiles and environment conditions have changed. Specifically, the detection threshold at the cluster head (denoted by T) is iteratively calibrated according to the feedback of the high-quality sensor, such that the system achieves the optimal detection performance. Our problem is formally formulated as follows.

PROBLEM 1. *To find a* stable *and* converging *calibration algorithm for the detection threshold T at the cluster head based on the feedback of high-quality sensor, such that the expected cost, i.e., $\mathbb{E}[c]$ which is given by (1), is minimized.*

We define *stability* and *convergence* based on control theories [Ogata 1995] as follows. The closed-loop system is *stable* if the system output $\mathbb{E}[c]$ is bounded given bounded inputs μ, σ^2 and S. Furthermore, the system *converges* if the system output $\mathbb{E}[c]$ converges to its theoretical minimum if all inputs are fixed. Moreover, in order to improve the real-time performance of the system, we expect that the output $\mathbb{E}[c]$ converges as soon as possible when the inputs have changed.

4.3. Approach Overview

Feedback control has been widely employed to improve the adaptability of systems [Adbelzaher et al. 2008]. In Problem 1, the system objective is to adapt to the unpredictable and dynamic changes of target profiles and physical environments. We face several challenges in implementing the closed-loop calibration. First, the relationship between the detection performance of low-end sensors and their stochastic measurements must be carefully considered to minimize the expected cost $\mathbb{E}[c]$. Second, the high-quality sensor should sleep for most of the time when no target is present due to its high energy consumption. We propose a calibration approach that features a feedback control loop to adaptively calibrate the detection threshold T, where the controller is implemented by the calibration algorithm located at the cluster head. The overview of our approach is as follows.

The detection threshold T is calibrated iteratively for every *calibration cycle*. Each calibration cycle comprises a number of detections. In each detection, the cluster head fuses the measurements received from the low-end sensors to make a decision by comparing against the current threshold T. Only if the cluster head makes a positive detection decision, the high-quality sensor is activated to make a detection and reports its decision to the cluster head. Such an on-demand activation scheme enables the high-quality sensor to sleep when no target is present. At the end of each calibration cycle, the cluster head estimates the detection performance of low-end sensors, which is characterized by the false alarm rate and missing probability, according to the detection history and the feedback of the high-quality sensor. The cluster head then calibrates the detection threshold T according to the difference between the estimated and the optimal detection performances.

In the rest of this paper, we first derive the closed-form expressions of the false alarm rate and missing probability of low-end sensors in Section 5. We then develop an adaptive calibration algorithm based on feedback control theory in Section 6. We analyze the impacts of communication performance on our algorithm in Section 7. Moreover, we extend our approach to address unknown target appearance probability and decision fusion in Section 8.

5. PERFORMANCE MODELING

In this section, we first derive the theoretical expressions of the system false alarm rate and missing probability of low-end sensors. We then derive the estimators of the two probabilities based on the feedback of the high-quality sensor.

5.1. Detection Performance of Low-end Sensors

We now derive the false alarm rate and missing probability of low-end sensors. Recall the distributions of $Y|H_0$ and $Y|H_1$ that are derived in Appendix A, i.e., $Y|H_0 \sim \mathcal{N}(\mu, \sigma^2)$ and $Y|H_1 \sim \mathcal{N}(\mu + S, \sigma^2)$. The system false alarm rate and missing probability of low-end sensors (denoted by P_{FL} and P_{ML}) are given by $P_{FL} = \mathbb{P}(Y \geq T|H_0) = Q\left(\frac{T-\mu}{\sigma}\right)$ and $P_{ML} = \mathbb{P}(Y \leq T|H_1) = Q\left(-\frac{T-\mu-S}{\sigma}\right)$, respectively, where $Q(\cdot)$ is the complementary cumulative distribution function of the standard normal distribution, i.e., $Q(x) = \int_{t=x}^{+\infty} \frac{1}{\sqrt{2\pi}} \exp\left(-\frac{t^2}{2}\right) \mathrm{d}t$. We now investigate the relationship between P_{FL} and P_{ML} when the expected cost $\mathbb{E}[c]$ is minimized which is the objective of Problem 1. Let $Q^{-1}(\cdot)$ denote the inverse function of $Q(\cdot)$. We have the following lemma.

LEMMA 5.1. *The expected cost $\mathbb{E}[c]$ is minimized if and only if $V = \delta$, where $V = \left(Q^{-1}(P_{FL})\right)^2 - \left(Q^{-1}(P_{ML})\right)^2$ and δ is given by (3).*

PROOF. From the expressions of P_{FL} and P_{ML}, we have

$$V = \left(Q^{-1}(P_{FL})\right)^2 - \left(Q^{-1}(P_{ML})\right)^2 = \left(\frac{T-\mu}{\sigma}\right)^2 - \left(-\frac{T-\mu-S}{\sigma}\right)^2 = \frac{2S}{\sigma^2} \cdot T - \frac{2\mu S + S^2}{\sigma^2}. \quad (4)$$

As discussed in Section 4.2, $\mathbb{E}[c]$ is minimized if and only if $T = T_{\mathrm{opt}}$, where T_{opt} is given by (2). By replacing T in (4) with T_{opt}, we have $V = \delta$. Moreover, as V is a linear function of T, $\mathbb{E}[c]$ is minimized if and only if $V = \delta$. □

We note that δ is a known constant which is independent of the unknown variables μ, σ^2 and S. From Lemma 5.1, Problem 1 can be reduced to the following problem.

PROBLEM 2. *To find the* stable *and* converging *calibration algorithm for the detection threshold T at the cluster head based on the feedback of high-quality sensor, such that $V = \delta$, where $V = \left(Q^{-1}(P_{FL})\right)^2 - \left(Q^{-1}(P_{ML})\right)^2$ and δ is given by (3).*

In Section 6, we will develop a calibration algorithm based on feedback control theory to solve Problem 2.

5.2. Feedback of High-quality Sensor

The objective of system detection performance defined in Problem 2 is to ensure $V = \delta$ where V is computed by P_{FL} and P_{ML}. In this section, we derive the estimators of P_{FL} and P_{ML} based on the detection history of low-end sensors and the feedback from the high-quality sensor.

Suppose each calibration cycle comprises m detections. The low-end sensors fuse their measurements to make a detection for every D seconds such that each sensor can sample at least one measurement when the target is present. Note that D is the lower bound of target appearance time. At the end of a calibration cycle, the cluster head counts the numbers of positive and negative decisions made by the high-quality sensor and estimates P_{FL} and P_{ML} based on the counts. As discussed in Section 4.1, the high-quality sensor may make wrong decisions, quantified by the false alarm rate (P_{FH}) and missing probability (P_{MH}), respectively. Therefore, our estimators account for the inaccuracy of the high-quality sensor.

We define the following notation subject to a calibration cycle: 1) n_{f1} and n_{d1} are the numbers of false alarms and correct detections made by the cluster head, respectively, which are unknown; 2) n_{f2} and n_{d2} are the numbers of positive decisions made by the cluster head but regarded to be false alarms and correct detections by the high-quality sensor, respectively, which can be counted by the cluster head. We have the following equations,

$$n_{f2} \simeq n_{f1}(1 - P_{FH}) + n_{d1}P_{MH}, \quad n_{d2} \simeq n_{f1}P_{FH} + n_{d1}(1 - P_{MH}).$$

where $n_{f1}(1 - P_{FH})$ represents the number of false alarms that are correctly identified by the high-quality sensor; $n_{d1}P_{MH}$ represents the number of correct detections that are wrongly classified as false alarms; $n_{f1}P_{FH}$ represents the number of false alarms that are wrongly classified as correct detections; $n_{d1}(1 - P_{MH})$ represents the number of detections that are correctly identified. From the above equations, the unknown n_{f1} and n_{d1} can be estimated as

$$n_{f1} \simeq \frac{n_{f2}(1 - P_{MH}) - n_{d2}P_{MH}}{1 - P_{FH} - P_{MH}}, \quad n_{d1} \simeq \frac{n_{d2}(1 - P_{FH}) - n_{f2}P_{FH}}{1 - P_{FH} - P_{MH}}.$$

Therefore, the estimates of P_{FL} and P_{ML}, denoted by $\widetilde{P}_{FL}$ and $\widetilde{P}_{ML}$, are given by:

$$\widetilde{P}_{FL} = \frac{n_{f1}}{m - m \cdot P_a}, \quad \widetilde{P}_{ML} = \frac{m \cdot P_a - n_{d1}}{m \cdot P_a}. \tag{5}$$

Note that $m \cdot P_a$ is the expected number of target appearances in a calibration cycle. The major errors of the above estimates are caused by the difference between the mean value $m \cdot P_a$ and the true number of target appearances which is a binomial random variable. According to the error analysis in Appendix B, the relative estimation errors of (5) are $\mathcal{O}\left(\frac{1}{\sqrt{m}}\right)$. Hence, as discussed in Appendix B, we can choose m to achieve any required estimation accuracy. The impact of m on the calibration performance is also evaluated in Section 10.2.1.

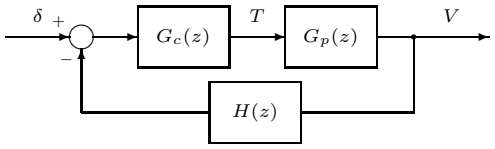

Fig. 2. The closed-loop system for minimizing $\mathbb{E}[c]$, where $G_c(z)$, $G_p(z)$ and $H(z)$ represent the transfer functions of the calibration algorithm, the system of low-end sensors and the feedback of the high-quality sensor, respectively.

6. ADAPTIVE CALIBRATION ALGORITHM

In this section, we first derive the control law for Problem 2 based on feedback control theory. We then implement it as an adaptive calibration algorithm.

6.1. Control Law

The objective of Problem 2 is to ensure $V = \delta$, where V is a function of the detection threshold T given by (4) and can be estimated based on the feedback of the high-quality sensor as discussed in Section 5.2. Moreover, the detection threshold T is calibrated for every calibration cycle. Therefore, Problem 2 is a typical discrete-time control problem [Ogata 1995], in which δ is the *reference*, T is the *control input* and V is the *controlled variable*. The block diagram of the feedback control loop is shown in Fig. 2, where $G_c(z)$, $G_p(z)$ and $H(z)$ represent the transfer functions of the calibration algorithm (i.e., controller), the system of low-end sensors and the feedback of the high-quality sensor, respectively.

We now derive the expressions of $G_p(z)$ and $H(z)$, and design $G_c(z)$ to solve Problem 2. By taking z-transform [Ogata 1995] to (4), we get the transfer function $G_p(z)$ as $G_p(z) = \frac{2S}{\sigma^2}$. At the end of a calibration cycle, the cluster head estimates V based on the feedback of the high-quality sensor as discussed in Section 5.2. Accordingly, the feedback of the high-quality sensor will take effect in the next calibration cycle. Therefore, the $H(z)$ has a component of z^{-1} that represents a delay of one calibration cycle. As discussed in Section 5.2, we can ignore the inaccuracy in estimating V if m is large. Hence, we adopt $H(z) = z^{-1}$. As the system to be controlled, i.e., $G_p(z)$, is a zero-order system, a first-order controller is sufficient to achieve the stability and convergence of the closed-loop system [Ogata 1995]. Hence, we let $G_c(z)$ be

$$G_c(z) = \frac{a}{1 - b \cdot z^{-1}}, \tag{6}$$

where $a > 0$ and $b > 0$. The coefficients a and b should be chosen to ensure system stability and convergence. In Section 6.2, we will discuss how to determine a and b based on stability and convergence analyses.

6.2. Stability and Convergence Analyses

We first analyze the system stability. The closed-loop transfer function, denoted by $T_c(z)$, is given by $T_c(z) = \frac{G_c(z)G_p(z)}{1+G_c(z)G_p(z)H(z)} = \frac{\frac{2aS}{\sigma^2} \cdot z}{z-\left(b-\frac{2aS}{\sigma^2}\right)}$. The closed-loop system has a pole at $z = b - \frac{2aS}{\sigma^2}$. From control theory [Ogata 1995], if the pole is within the unit circle centered at the origin, i.e., $\left|b - \frac{2aS}{\sigma^2}\right| < 1$, the system is stable. Therefore, the sufficient condition for stability is $\frac{\sigma^2}{2S}(b-1) < a < \frac{\sigma^2}{2S}(b+1)$.

We then analyze the steady-state error of the system. The open-loop transfer function, denoted by $T_o(z)$, is given by $T_o(z) = G_c(z)G_p(z)H(z) = \frac{2aS}{\sigma^2(z-b)}$. By letting $b = 1$, the system is a type I system [Ogata 1995], of which the controlled variable V can converge to the reference δ provided that the system is stable. Therefore, by replacing

b with 1, the condition for both stability and convergence is $0 < a < \frac{\sigma^2}{S}$. Accordingly, only a is left to be determined.

Finally, we discuss the transient response of the system, which characterizes how fast the closed-loop system converges. There exists a fundamental trade-off between the stability and transient response performance [Ogata 1995]. Particularly for our problem, the system converges faster for larger a at the price of worse system stability. Therefore, the best setting for a is a value close to the upper bound $\frac{\sigma^2}{S}$. However, σ^2 and S are often unknown and changeable at run time as discussed in Section 4.2. We now propose an approach to adaptively estimate the upper bound $\frac{\sigma^2}{S}$. The details are as follows.

From (4), the control input T and the controlled variable V have a linear relationship with slope of $K = \frac{2S}{\sigma^2}$. We employ the exponential moving average [NIST/SEMATECH 2010] to estimate and update the slope K. Specifically, in the k^{th} calibration cycle, the slope K is estimated as $K = \frac{V[k-1]-V[k-2]}{T[k-1]-T[k-2]}$, where $T[k-1]$ is the detection threshold set by the calibration algorithm in the $(k-1)^{\text{th}}$ calibration cycle, and $V[k-1]$ is the corresponding output of low-end sensors. We note that $V[k-1]$ is obtained in the k^{th} calibration cycle due to the delay of feedback. The exponential moving average of K in the k^{th} calibration cycle, denoted by $\overline{K}[k]$, is updated by $\overline{K}[k] = (1-\alpha)\cdot\overline{K}[k-1]+\alpha\cdot K$, where α is a weight in $(0,1)$. Note that the moving average $\overline{K}$ can quickly adapt to the change of K by setting a large α. However, doing so reduces the algorithm robustness to errors such as the inaccuracy in estimating V. The upper bound $\frac{\sigma^2}{S}$ is estimated as $\frac{\sigma^2}{S} = \frac{2}{\overline{K}[k]}$ and a is set to be $\beta \cdot \frac{2}{\overline{K}[k]}$, where β is a coefficient in $(0,1)$. Note that β is set to be 0.5 in the experiments conducted in this paper. The $\overline{K}[0]$ can be set to be a large enough value such that the system is stable initially.

6.3. Adaptive Calibration Algorithm

In this section, we implement the control law derived in Section 6.1 in time domain. According to Fig. 2, we have $G_c(z) = \frac{T(z)}{\delta - H(z)V(z)}$. By replacing $G_c(z)$ with (6) and $H(z) = z^{-1}$, we have $T(z) = b\cdot z^{-1}T(z)+a\cdot\big(\delta - z^{-1}V(z)\big)$ and its implementation in time domain is $T[k] = b\cdot T[k-1] + a\cdot(\delta - V[k-1])$, where $V[k-1] = \Big(Q^{-1}(\widetilde{P}_{FL})\Big)^2 - \Big(Q^{-1}(\widetilde{P}_{ML})\Big)^2$, $T[k-1]$ and $T[k]$ are the detection thresholds in the $(k-1)^{\text{th}}$ and k^{th} calibration cycle, respectively. The estimates $\widetilde{P}_{FL}$ and $\widetilde{P}_{ML}$ are computed using (5) when the detection threshold is $T[k-1]$. As discussed in Section 6.2, $b = 1$ and a is updated for each calibration cycle to ensure system stability and convergence.

7. IMPACT OF COMMUNICATION PERFORMANCE

The adaptive calibration algorithm in Section 6 is impacted by communication performance. In this section, we investigate the impacts caused by packet loss and feedback delay.

7.1. Packet Loss and Optimal Routing Algorithm

In this section, we first analyze the impact of packet loss in the wireless communication among low-end sensors, and then propose an optimal routing algorithm to minimize the impact. From the analysis in Section 6.1, the system stability is affected by the upper bound $\frac{\sigma^2}{S}$. We assume that the cluster head only fuses the received measurements. In the case of stochastic packet loss, both the aggregated signal energies and noise variances, i.e., S and σ^2, can change rapidly. The closed-loop system can become

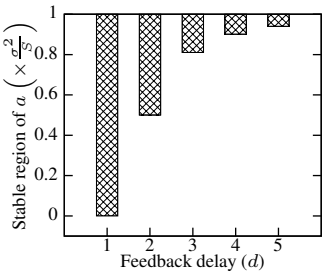

Fig. 3. The region of a for system stability under various d.

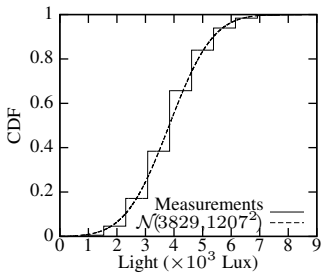

Fig. 4. The CDF of the fused readings from 5 motes.

unstable due to the rapid changes of S and σ^2. We study the impact of packet loss by investigating the relative deviations of S and σ^2, which characterize the magnitude of changes caused by stochastic packet loss. Let p_i denote the end-to-end packet reception rate (PRR) of the multi-hop path from sensor i to the cluster head. We assume that $p_i \in [0.5, 1]$. Let $u_i \in \{0, 1\}$ denote the packet delivery state of sensor i in a transmission, which is a Bernoulli random variable with success probability of p_i. In the presence of packet loss, $S = \sum_{i=1}^{N} s_i u_i$. We assume that s_i has non-zero lower and upper bounds, denoted by $s_{\min}$ and $s_{\max}$, respectively. Hence, we have $\mathbb{E}[S] = \sum_{i=1}^{N} s_i \mathbb{E}[u_i] = \sum_{i=1}^{N} s_i p_i \geq \frac{N \cdot s_{\min}}{2}$ and $\mathrm{Var}[S] = \sum_{i=1}^{N} s_i^2 \mathrm{Var}[u_i] = \sum_{i=1}^{N} s_i^2 p_i (1 - p_i) \leq \frac{N \cdot s_{\max}^2}{4}$. The relative standard deviation (RSD) [NIST/SEMATECH 2010] of S satisfies $\mathrm{RSD}(S) = \frac{\sqrt{\mathrm{Var}[S]}}{\mathbb{E}[S]} \leq \frac{s_{\max}}{s_{\min}} \cdot \frac{1}{\sqrt{N}}$, i.e., $\mathrm{RSD}(S) = \mathcal{O}\left(\frac{1}{\sqrt{N}}\right)$. Therefore, the impact of packet loss can be mitigated by deploying more low-end sensors subject to allowable communication throughput. The derivation of $\mathrm{RSD}(\sigma^2)$ is similar and hence omitted here.

We now propose an optimal routing algorithm that minimizes $\mathrm{RSD}(S)$. As $\frac{\partial \mathbb{E}[S]}{\partial p_i} > 0$ and $\frac{\partial \mathrm{Var}[S]}{\partial p_i} \leq 0$ for $p_i \in [0.5, 1]$, $\frac{\partial \mathrm{RSD}(S)}{\partial p_i} \leq 0$. Therefore, $\mathrm{RSD}(S)$ is minimized when each p_i is maximized separately. Let R_i denote the routing path from sensor i to the cluster head and $p(h)$ denote the PRR of hop $h \in R_i$. Accordingly, $p_i = \prod_{\forall h \in R_i} p(h)$ and the optimal routing path that maximizes p_i is given by $\mathrm{argmin}_{R_i} \sum_{\forall h \in R_i} -\log p(h)$, i.e., the shortest path from sensor i to the cluster head where the cost of hop h is $-\log p(h)$. In Section 10.2.2, we will evaluate the impact of packet loss as well as various routing algorithms on the performance of the calibration algorithm.

7.2. Impact of Feedback Delay

In this section, we analyze the impact of feedback delay on system stability. Suppose the feedback is delayed for d calibration cycles where d is an unknown integer. Therefore, the transfer function of the feedback is $H(z) = z^{-d}$. Several practical issues can attribute to the feedback delay, such as the communication delay due to the low duty cycle of sensors. We adopt a widely used technique called the Jury test [Ogata 1995] to analyze the stability of our algorithm. The details can be found in Appendix C. Fig. 3 plots the regions of a in (6) for system stability when d is from 1 to 5. We can see from the figure that the stability condition becomes more critical for larger d. This is consistent with the intuition in control theory that the system stability decreases with the delay in the closed-loop. In Section 10.2.2, we will evaluate the impact of d on the performance of the calibration algorithm. The result shows that the feedback delay has little impact on the performance of our calibration algorithm when d is up to 10.

8. EXTENSIONS

We now discuss several open issues that have not been addressed in previous sections and extend our approach to address them.

8.1. Handling Unknown and Changeable Target Appearance Probability

In previous sections, we assume that the target appearance probability, i.e., P_a, is a known constant. However, in practice, the estimated P_a may be inaccurate. Moreover, P_a can change rapidly in many applications. The optimal solution for detecting targets with variable prior probabilities is still an open issue in detection theory [Varshney 1996; Duda et al. 2001]. In this section, we employ a sub-optimal detection criterion called *minimax* criterion [Duda et al. 2001], which is widely adopted to handle unknown and changeable prior probabilities. According to the Bayesian detection theory, the optimal $\mathbb{E}[c]$ is a concave function of P_a. The minimax detector is designed according to the P_a for which the optimal $\mathbb{E}[c]$ is maximum (i.e., worst case). Moreover, as an important property of minimax detector, its $\mathbb{E}[c]$ is a constant with respect to P_a. Hence, the performance of minimax detector would not downgrade when P_a changes rapidly. In contrast, the performance of an optimal detector can deteriorate significantly when P_a has changed [Duda et al. 2001]. The condition of minimax detector is $(C_{00} - C_{11}) + (C_{10} - C_{00})P_{FL} - (C_{01} - C_{11})P_{ML} = 0$ [Duda et al. 2001]. Note that P_{FL} and P_{ML} are the false alarm rate and missing probability of low-end sensors, which are derived in Section 5.1. The above condition has a closed-form solution with respect to the detection threshold T if and only if $C_{00} = C_{11}$ and $C_{01} = C_{10}$. In such a case, the above condition reduces to $P_{FL} = P_{ML}$. In particular, we focus on the special case of $C_{00} = C_{11} = 0$ and $C_{01} = C_{10} = 1$, where the expected cost $\mathbb{E}[c]$ represents the average error rate. The general case of expected cost is left for our future work. We can extend our approach presented in previous sections to achieve minimax error rate when P_a is unknown and changeable. The major changes are summarized as follows:

— To satisfy the condition of minimax error rate, i.e., $P_{FL} = P_{ML}$, the *controlled variable* can be $V = Q^{-1}(P_{FL}) - Q^{-1}(P_{ML})$ and hence the *reference* is zero. Moreover, it is easy to derive the relationship between the controlled variable V and the control input T, which is $V = \frac{2}{\sigma} \cdot T - \frac{2\mu+S}{\sigma}$. Therefore, the transfer function of the system of low-end sensors is $G_p(z) = \frac{2}{\sigma}$.

— In (5), the calculations of $\widetilde{P}_{FL}$ and $\widetilde{P}_{ML}$ require the estimate of the number of target appearances in a calibration cycle (i.e., $m \cdot P_a$). Due to the unknown P_a, it is difficult to accurately estimate the number of target appearances if the high-quality sensor is activated only when the low-end sensors make a positive decision. We now discuss the basic idea to handle this issue. In addition to being triggered by low-end sensors, the high-quality sensor can be periodically activated during a calibration cycle. Suppose the high-quality sensor is activated for n_a times during a calibration cycle, in which the high-quality sensor makes n_p positive decisions. Let n_1 denote the number of target appearances when the high-quality sensor is activated. We have $n_p \simeq (n_a - n_1) \cdot P_{FH} + n_1 \cdot (1 - P_{MH})$. Hence, n_1 is given by $n_1 \simeq \frac{n_p - n_a \cdot P_{FH}}{1 - P_{FH} - P_{MH}}$ and the number of target appearances during the current calibration cycle can be estimated as $\frac{n_1}{n_a} \cdot m$, where m is the number of detections in a calibration cycle. The accuracy of the estimate can be improved if the high-quality sensor is activated more frequently, i.e., a larger n_a. However, frequently activating the high-quality sensor will lead to high energy consumption. We define the *extra utilization* of high-quality sensor as $\frac{n_a}{m}$, which characterizes the extra overhead caused by estimating the number of target appearances. We will evaluate the impact of extra utilization of high-quality sensor on the system detection performance in Section 10.2.3. The result shows that the

system detection performance does not degrade even when the extra utilization is as low as $\frac{1}{10}$.

— Following the analyses in Section 6.2, the condition for stability and convergence can be derived as $0 < a < \sigma$ and $b = 1$. The approach that adaptively estimates the upper bound of a is still applicable.

The extended approach described above is evaluated in Section 10.2.3. The results show that this approach is robust to rapidly changing P_a.

8.2. Decision Fusion

In this section, we extend our approach to a decision fusion model. Different from the value fusion model adopted in previous sections, decision fusion operates in a distributed manner. Specifically, each sensor makes a *local* decision based on its measurements and transmits its decision to the cluster head, which makes a *system* decision according to the local decisions. Due to its low communication overhead, decision fusion is often preferred in bandwidth-constrained CPS and sensor systems.

However, a key challenge for employing the decision fusion model is the complexity in the analysis of system detection performance. It is proved in [Chair and Varshney 1986] that the optimal test statistics at the cluster head is the weighted sum of local decisions where the weights are determined by the local detection performance of sensors. However, there is no closed-form formula for characterizing the system detection performance under such a model. Moreover, as discussed in [Niu and Varshney 2005], the optimal decision fusion model is infeasible when sensors have little information about their detection performance. In this section, we will employ the equal gain combining model which has been widely adopted in previous literature [Varshney 1996; Niu and Varshney 2005; Tan et al. 2008; 2010] and analyze the approximate system detection performance. Specifically, sensor i makes the local decision by comparing its measurement y_i against a local threshold t_i. If $y_i \geq t_i$, it decides 1; otherwise, it decides 0. Let I_i denote the local decision of sensor i. The test statistics at the cluster head is the sum of local decisions, i.e., $Y = \sum_{i=1}^{N} I_i$. The system decision is made by comparing Y against the threshold T. In this section, we also assume that the target appearance probability P_a is unknown and changeable. Therefore, our objective is to find the *stable* and *converging* calibration algorithm for the detection thresholds, $\{t_1, t_2, \ldots, t_N, T\}$, such that the system has minimax error rate.

We first analyze the detection performance of the decision fusion model. Let α_i and β_i denote the false alarm rate and missing probability of sensor i, respectively. In the absence of target, the local decision of sensor i, $I_i|H_0$, follows the Bernoulli distribution with α_i as success probability. As $\{I_i|H_0, i \in [1, N]\}$ are mutually independent, the mean and variance of $Y|H_0$ are given by $\mathbb{E}[Y|H_0] = \sum_{i=1}^{N} \mathbb{E}[I_i|H_0] = \sum_{i=1}^{N} \alpha_i$ and $\mathrm{Var}[Y|H_1] = \sum_{i=1}^{N} \mathrm{Var}[I_i|H_0] = \sum_{i=1}^{N} \alpha_i - \sum_{i=1}^{N} \alpha_i^2$, respectively. However, $\{I_i|H_0, i \in [1, N]\}$ are not identically distributed. We have proved the condition of Lyapunov's central limit theorem [Ash and Doléans-Dade 1999] for a finite sequence of independent Bernoulli random variable in [Tan et al. 2008; 2010]. According to the Lyapunov's central limit theorem, $Y|H_0$ follows the normal distribution when N is large, i.e., $Y|H_0 \sim \mathcal{N}\left(\sum_{i=1}^{N} \alpha_i, \sum_{i=1}^{N} \alpha_i - \sum_{i=1}^{N} \alpha_i^2\right)$. Similarly, we can derive the distribution of Y in the presence of target, i.e., $Y|H_1 \sim \mathcal{N}\left(\sum_{i=1}^{N}(1-\beta_i), \sum_{i=1}^{N}(1-\beta_i) - \sum_{i=1}^{N}(1-\beta_i)^2\right)$. Therefore, the system false alarm rate and missing probability can be approximated by $P_{FL} \simeq Q\left(\frac{T - \sum_{i=1}^{N} \alpha_i}{\sqrt{\sum_{i=1}^{N} \alpha_i - \sum_{i=1}^{N} \alpha_i^2}}\right)$ and $P_{ML} \simeq Q\left(-\frac{T - \sum_{i=1}^{N}(1-\beta_i)}{\sqrt{\sum_{i=1}^{N}(1-\beta_i) - \sum_{i=1}^{N}(1-\beta_i)^2}}\right)$.

We now discuss how to achieve minimax error rate under the decision fusion model. As discussed in Section 8.1, the condition of minimax error rate is $P_{FL} = P_{ML}$. By solving $P_{FL} = P_{ML}$, the optimal threshold at the cluster head, T_{opt}, is

$$T_{\text{opt}} = \frac{\mathbb{E}[Y|H_0] \cdot \sqrt{\text{Var}[Y|H_1]} + \mathbb{E}[Y|H_1] \cdot \sqrt{\text{Var}[Y|H_0]}}{\sqrt{\text{Var}[Y|H_0]} + \sqrt{\text{Var}[Y|H_1]}}. \tag{7}$$

Therefore, the T_{opt} can be computed as long as $\{\alpha_i, \beta_i | i \in [1, N]\}$ are given. Denote $\boldsymbol{\alpha} = [\alpha_1, \ldots, \alpha_N]^{\text{T}}$, $\boldsymbol{\beta} = [\beta_1, \ldots, \beta_N]^{\text{T}}$ and $\mathbf{1} = [1, \ldots, 1]^{\text{T}}$. When $T = T_{\text{opt}}$, the average error rate, denoted by P_E, is $P_E = P_{FL} = Q(f(\boldsymbol{\alpha}, \boldsymbol{\beta}))$ [Duda et al. 2001], where $f(\boldsymbol{\alpha}, \boldsymbol{\beta}) = \frac{(\mathbf{1}-\boldsymbol{\beta})^{\text{T}}\mathbf{1} - \boldsymbol{\alpha}^{\text{T}}\mathbf{1}}{\sqrt{\boldsymbol{\alpha}^{\text{T}}\mathbf{1} - \boldsymbol{\alpha}^{\text{T}}\boldsymbol{\alpha}} + \sqrt{(\mathbf{1}-\boldsymbol{\beta})^{\text{T}}\mathbf{1} - (\mathbf{1}-\boldsymbol{\beta})^{\text{T}}(\mathbf{1}-\boldsymbol{\beta})}}$. As $Q(\cdot)$ is a decreasing function, if $f(\boldsymbol{\alpha}, \boldsymbol{\beta})$ is maximized, P_E will be further minimized. However, it is difficult to analytically maximize $f(\boldsymbol{\alpha}, \boldsymbol{\beta})$ due to its complex expression. The Monte Carlo simulations show that $f(\boldsymbol{\alpha}, \boldsymbol{\beta})$ decreases with $\sum_{i=1}^{N}(\alpha_i + \beta_i)$ with a high probability ($> 98\%$). The details of the simulations can be found in Appendix D. Therefore, in practice, $f(\boldsymbol{\alpha}, \boldsymbol{\beta})$ can be maximized by minimizing $\sum_{i=1}^{N}(\alpha_i + \beta_i)$. As a result, if $\alpha_i + \beta_i$ is minimized for each sensor i separately, P_E is minimized. Note that $\alpha_i = Q\left(\frac{t_i - \mu_i}{\sigma_i}\right)$, $\beta_i = Q\left(-\frac{t_i - \mu_i - s_i}{\sigma_i}\right)$, and $\alpha_i + \beta_i$ is minimized only if $\alpha_i = \beta_i$. Therefore, by running the controller proposed in Section 8.1 at each local sensor, $\alpha_i + \beta_i$ can be minimized for each sensor i. Moreover, by setting the detection threshold at the cluster head according to (7) using the estimated $\{\alpha_i, \beta_i | i \in [1, N]\}$, the minimax error rate can be achieved. In Section 10.2.3, we will conduct comparative simulations to evaluate the system performance under the value and decision fusion models, respectively.

9. TESTBED EXPERIMENTS

To evaluate the performance of our adaptive calibration approach, we have conducted both experiments on a testbed of Tmotes as well as extensive trace-driven simulations based on real data traces. The small-scale testbed experiments account for many practical issues such as sensor's duty cycle and hence verify the feasibility of our approach. The trace-drive simulations allow us to extensively evaluate our approach in a wide range of settings such as noise level and communication performance. We first present the testbed experiments in this section and then the trace-driven simulations in Section 10.

9.1. Experiment Methodology and Settings

In our experiments, five Tmotes [Moteiv Corp. 2006] are attached against the LCD screen of a desktop computer to detect a light spot displayed on the LCD. The light spot simulates the target that randomly appears, and its display is controlled by a program. We note that such an experimental methodology is also employed in previous works [Hwang et al. 2007]. The system objective is to adapt to the intensity change of the light spot that randomly appears in each time slot with a probability of $P_a = 50\%$. The length of a time slot is one second. The motes measure light intensity for every 250 milliseconds via the on-board Hamamatsu S1087-01 light sensors [Moteiv Corp. 2006] and transmit the measurements to the sink node that is connected to a laptop computer. Note that the motes are not synchronized. NesC language is used to program the motes, and Java is used to implement the calibration algorithms that run on the laptop. The sink fuses the readings received within every 250 milliseconds and detects the light spot. A webcam is attached against the LCD and used as the high-quality sensor. When the webcam is triggered by the sink to make a detection, it computes the average intensity over all pixels and makes the detection decision by

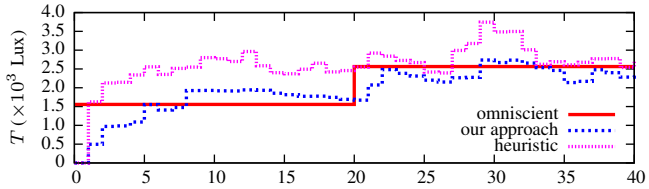

(a) Detection threshold T *vs.* index of calibration cycle.

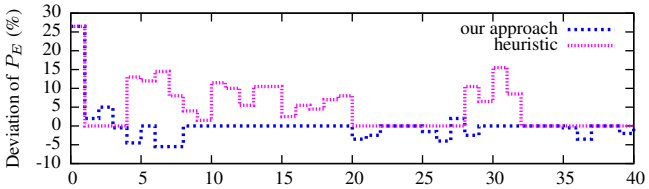

(b) Deviation of P_E with respect to the omniscient approach *vs.* index of calibration cycle.

Fig. 5. Convergence of various calibration approaches.

comparing against a threshold. The threshold is set to be 175 in our experiments. The webcam's false alarm rate and missing probability, i.e., P_{FH} and P_{MH}, are 3.3% and 1.4%, respectively, which are estimated offline. The length of a calibration cycle, i.e., m, is 200 detections. The detection threshold T at the sink is initially set to be zero. We let $C_{00} = C_{11} = 0$ and $C_{10} = C_{01} = 1$. Hence, the cost metric given by (1) is the average error rate of the motes, which is denoted by P_E.

We employ a *heuristic* calibration approach as the baseline, in which the webcam is also activated to make a detection when the cluster head makes a positive decision. The heuristic approach sets the detection threshold according to the S, μ and σ^2 that are estimated from noisy measurements of low-end sensors. The details of the heuristic approach are as follows. Let $\widetilde{H}_0'$ and $\widetilde{H}_1'$ represent the negative and positive detection decisions of the webcam, respectively. The mean and variance of the fused noise, i.e., μ and σ^2, are estimated as $\mathbb{E}[Y|\widetilde{H}_0 \vee (\widetilde{H}_1 \wedge \widetilde{H}_0')]$ and $\mathrm{Var}[Y|\widetilde{H}_0 \vee (\widetilde{H}_1 \wedge \widetilde{H}_0')]$, respectively. The aggregated signal energies is estimated as $S = \mathbb{E}[Y|\widetilde{H}_1 \wedge \widetilde{H}_1'] - \mu$. The detection threshold is then set according to the optimal formula (2) with the estimated S, μ and σ^2. The heuristic calibration approach is a typical way to use the feedback of the high-quality sensor. However, it does not exploit the relationship between the detection performance of low-end sensors and their stochastic measurements.

9.2. Experiment Results

We first evaluate the sensor measurements. Fig. 4 plots the cumulative distribution functions (CDFs) of the fused measurement when the light spot is present as well as the normal distribution $\mathcal{N}(3829, 1207^2)$, respectively. We note that the fused measurement is a discrete random variable. We can see from Fig. 4 that the distribution of the fused measurement can be approximated by the normal distribution, which is consistent with the assumptions in Section 3.

We then evaluate the convergence of the calibration approaches. Fig. 5(a) plots the evolution of the detection thresholds calibrated by various approaches. The *omniscient* approach computes the optimal detection threshold using (2) based on the S, μ and σ^2 that are estimated in extra offline experiments. At the 20^{th} calibration cycle, we increase the intensity of the light spot to evaluate the adaptability of the calibration approaches. As P_E is the cost metric, Fig. 5(b) plots the deviation of P_E from that of the

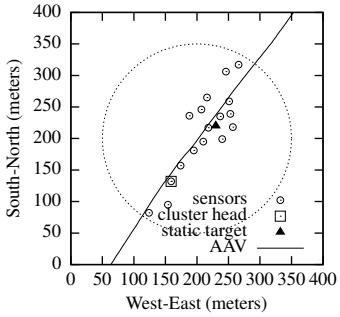

Fig. 6. Sensor deployment and the trajectory of AAV.

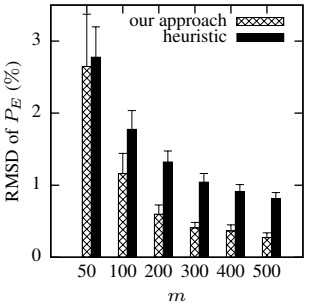

Fig. 7. The RMSD of P_E with respect to the omniscient approach *vs.* m.

omniscient approach. From Fig. 5(a) and 5(b), we can see that our approach converges to the optimal results after 8 calibration cycles. Moreover, our approach can respond to the target change within 3 calibration cycles. In contrast, the heuristic approach has considerably large deviations from the optimal results. Specifically, in Fig. 5(a), the average relative errors of our approach and the heuristic approach after the 10^{th} calibration cycle are 12.8% and 30.5%, respectively.

10. TRACE-DRIVEN SIMULATIONS

In addition to the testbed experiments, we also conduct trace-driven simulations to extensively evaluate the performance of our calibration approach.

10.1. Simulation Methodology and Settings

We use the real data traces collected in the DARPA SensIT vehicle detection experiment [Duarte and Hu 2004], where 75 WINS NG 2.0 nodes are deployed to detect Amphibious Assault Vehicles (AAVs) driving through a road section. We refer to [Duarte and Hu 2004] for detailed setup of the experiment. The dataset used in our simulations includes the ground truth data and the acoustic time series recorded by 17 nodes at a frequency of 4960 Hz. The ground truth data include the positions of sensors and the trajectory of the AAV recorded by a GPS device. Fig. 6 [Duarte and Hu 2004] shows the sensor deployment and the trajectory of an AAV run. In order to evaluate the calibration algorithms in the case of changing noise level, we first let the target appears at a fixed location shown in Fig. 6. A sensor's measurement is set to be the real measurement when the AAV is closest to the fixed location. Besides the case of static target, we also evaluate our approach in detecting the moving target, where the whole data traces are used. The AAV is regarded to be present when it is in the circular region shown in Fig. 6. As it often takes tens of seconds for the AAV to drive through the road section in Fig. 6, the sampling period of the sensors, i.e., D, is set to be 15 seconds in the simulations. The target appearance probability P_a is set to be 25% except those explicitly specified. As there is no extra high-quality sensor such as camera in the SensIT experiment, we use a pseudo camera in the simulations, which generates random detection results based on the ground truth data. The pseudo camera's false alarm rate and missing probability, i.e., P_{FH} and P_{MH}, are both set to be 1%.

10.2. Simulation Results

10.2.1. Convergence and Adaptability. In this set of simulations, we evaluate the convergence and adaptability of our calibration approach in the cases of changing noise and moving targets, respectively. Fig. 8(a) plots the detection thresholds calibrated by various approaches in detecting a static targets with changing noise level. The noise

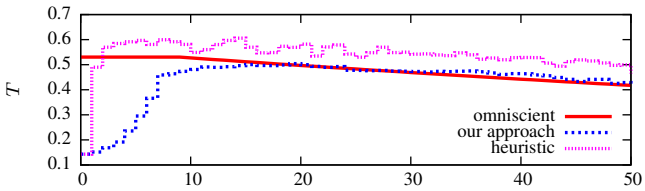

(a) Static target, changing noise level.

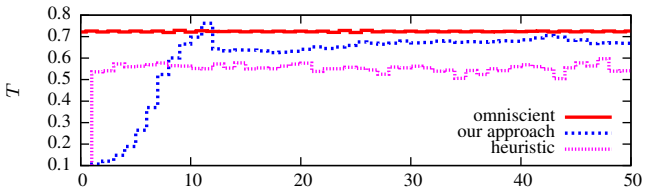

(b) Moving target, constant noise level.

Fig. 8. Detection threshold T *vs.* index of calibration cycle.

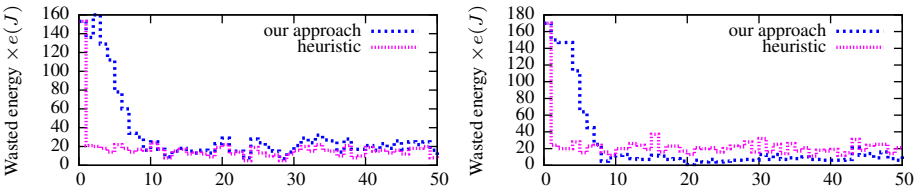

(a) Static target, changing noise level (b) Moving target, constant noise level

Fig. 9. Camera's wasted energy caused by false alarms *vs.* index of calibration cycle.

standard deviation of each sensor, i.e., σ_i, decreases by 4×10^{-4} in each calibration cycle from the 10^{th} calibration cycle. Fig. 8(b) plots the results of detecting moving targets. Note that calibrating the sensors for detecting moving target is challenging as the aggregated signal energies, i.e., S, significantly varies when the target is at different locations. In our experiment, the optimal detection threshold T_{opt} in each calibration cycle varies from 0.528 to 2.379 due to the changing S caused by the movement of the target. The detection threshold of the omniscient approach plotted in Fig. 8(b) is calculated using (2) where the S is computed as the average of the aggregated signal energies when the target is within the circular region shown in Fig. 6. From the figures, we can see that our approach converges to the optimal results after 10 calibration cycles and can adapt to changing noise level as well as moving target. Although the heuristic approach has short rise time, it has considerably large steady-state error.

We now evaluate the energy consumed by the camera in processing images triggered by false alarms. Suppose the camera consumes e Joules per target recognition task. Fig. 9 plots the camera's *wasted energy* caused by false alarms of the low-end sensors, which corresponds to the results shown in Fig. 8. We can see from the figure that the wasted energy drops to a low level when the system converges. The results show that, by taking advantage of the on-demand activation strategy, the calibrated system is effective in reducing the energy consumption of the high-quality sensor. As the detection threshold calibrated by the heuristic approach is higher than our approach in Fig. 8(a), the heuristic approach has fewer false alarms leading to less wasted energy as shown in Fig. 9(a). However, the error rate of the heuristic approach does not converge to its minimum due to the considerably large steady-state errors shown in Fig. 8(a). In

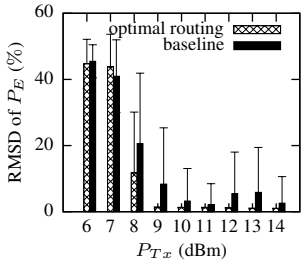

Fig. 10. $\mathrm{RMSD}(P_E)$ with respect to the omniscient approach *vs.* transmission power P_{Tx}.

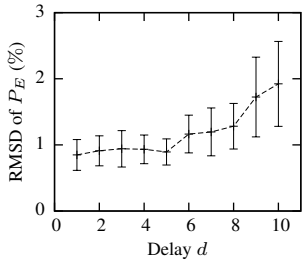

Fig. 11. $\mathrm{RMSD}(P_E)$ with respect to the omniscient approach *vs.* delay d.

Fig. 9(b), the heuristic approach incurs more wasted energy due to its lower detection threshold as shown in Fig. 8(b).

From the error analysis in Section 5.2, the number of detections in a calibration cycle, i.e., m, affects the accuracy of feedback. The second set of simulations evaluate the impact of m on the performance of our calibration algorithm. We employ the root mean square deviation (RMSD) of P_E with respect to the omniscient approach as the performance metric. Specifically, $\mathrm{RMSD}(P_E) = \sqrt{\mathbb{E}[(P_E - P_{E,\mathrm{opt}})^2]}$, where $P_{E,\mathrm{opt}}$ is the average error rate of the omniscient approach. Fig. 7 plots the RMSD of P_E versus m. The system shows better convergence for larger m, which is consistent with our analysis in Section 5.2. Moreover, our approach yields smaller RMSD of P_E than the heuristic approach under a wide range of m.

10.2.2. Impact of Communication Performance. In this set of simulations, we evaluate the impacts of packet loss and feedback delay that are analyzed in Section 7. We employ the link model in [Zuniga and Krishnamachari 2004] to compute the PRR of each link in the system. The routing path from each sensor to the cluster head (shown in Fig. 6) is computed by Dijkstra's algorithm. Besides the optimal routing algorithm proposed in Section 7.1, we employ a baseline routing algorithm in which the cost of link h is $\frac{1}{p(h)}$, where $p(h)$ is the PRR of link h. Such a metric is widely adopted to characterize the expected number of transmissions on a lossy link [Woo et al. 2003]. Fig. 10 plots the RMSD of P_E under various routing algorithms versus the transmission power P_{Tx} at each sensor. We can see from the figure that our approach with the optimal routing algorithm converges when the P_{Tx} is no lower than 9 dBm. However, the system shows considerably large deviation when the baseline routing algorithm is used. Fig. 11 plots the RMSD of P_E versus the feedback delay d. We can see that our calibration algorithm is robust to feedback delay. Specifically, the RMSD of P_E increases 1% even if the delay is 10 calibration cycles.

10.2.3. Handling Rapidly Changing P_a. We finally evaluate the minimax detection approaches that are proposed in Section 8 to handle unknown and changeable target appearance probability. In the simulations, the target appearance probability P_a is randomly chosen from $[0.1, 0.9]$ for each calibration cycle. Moreover, in order to evaluate the adaptability of the proposed approaches, the noise standard deviation of each sensor, i.e., σ_i, decreases by 4×10^{-4} in each calibration cycle from the 10^{th} calibration cycle. As discussed in Section 8.1, due to unknown P_a, extra camera activations are needed to estimate the number of target appearances so that we can compute the false alarm rate and missing probability. In the simulations, the camera is periodically activated for n_a times during each calibration cycle. Therefore, the extra camera utilization is $\frac{n_a}{m}$. Besides the minimax detection approaches proposed in Section 8, we employ an *online estimation* approach to study the impact of rapidly changing target

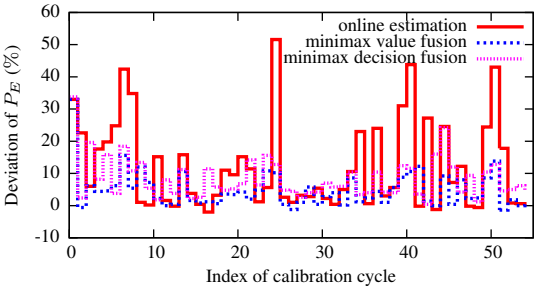

Fig. 12. Deviation of P_E with respect to the omniscient approach *vs.* index of calibration cycle. Extra camera utilization is $1/5$.

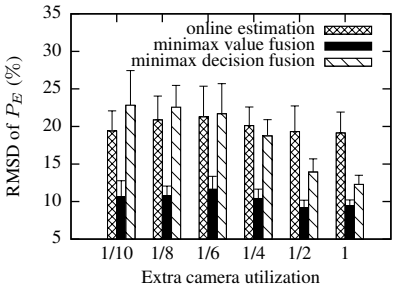

Fig. 13. RMSD of P_E with respect to the omniscient approach *vs.* extra camera utilization.

appearance probability on system detection performance. We assume that the online estimation approach can accurately estimate S, μ and σ^2. Moreover, it uses the P_a that is estimated from the extra camera activations in the previous calibration cycle to calculate the detection threshold for the current cycle using (2). Therefore, the estimated P_a can be significantly different from the true value due to the rapid change of P_a.

Fig. 12 plots the deviation of P_E from the omniscient approach. We can see that the detection performance of the online estimation approach varies significantly. This result is consistent with the conclusion in [Duda et al. 2001] that the performance of an optimal Bayesian detector based on inaccurate prior probabilities can deteriorate seriously. In contrast, we can see from Fig. 12 that the minimax approaches based on value fusion and decision fusion models show significantly less variance than the online estimation approach. Moreover, they achieve comparable detection performance. Fig. 13 plots the RMSD of P_E with respect to the omniscient approach versus the extra camera utilization. We can see that the detection performance of the online estimation approach and the value fusion-based minimax approach does not degrade when the extra camera utilization is as low as $1/10$. However, the error rate of the decision fusion-based minimax approach increases when camera utilization decreases. Therefore, value fusion is more robust to the inaccurate estimation of the number of target appearances in case of unknown P_a.

11. CONCLUSION

The performance of a CPS system composed of low-cost sensors is inevitably undermined by the physical uncertainties from sensor hardware, environment and the monitored physical process. In this paper, we focus on calibrating a class of CPS systems whose primary objective is to detect events or targets of interest. We propose an adaptive calibration approach that exploits sensor heterogeneity and features a feedback control loop to deal with these uncertainties. We develop a control-theoretical calibration algorithm that ensures provable system stability and convergence. We also systematically analyze the impacts of several communication issues such as communication reliability and delay, and propose an optimal routing algorithm that minimizes the impact of packet loss on system stability. Moreover, we extend our approach to address various data fusion models and rapidly changing dynamics of the monitored physical process. The experiment results on a testbed of Tmotes as well as extensive trace-driven simulations demonstrate that the calibrated system maintains the optimal detection performance in the presence of various system and environmental dynamics.

d	z^0	z^1	z^2	z^3
2	$\frac{2aS}{\sigma^2}$	-1	1	
3	$\frac{2aS}{\sigma^2}$	0	-1	1
	1	-1	0	$\frac{2aS}{\sigma^2}$
	$\left(\frac{2aS}{\sigma^2}\right)^2 - 1$	1	$-\frac{2aS}{\sigma^2}$	

Fig. 14. Jury stability tables for $d = 2$ and $d = 3$.

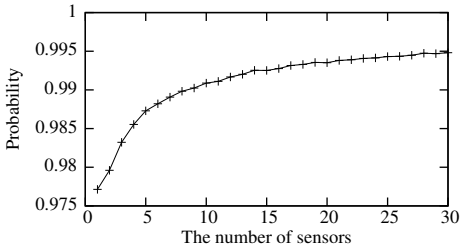

Fig. 15. The probability that $f(\boldsymbol{\alpha}, \boldsymbol{\beta})$ decreases with $\sum_{i=1}^{N}(\alpha_i + \beta_i)$ versus the number of sensors.

APPENDIX

A. OPTIMAL BAYESIAN DETECTOR

The optimal decision rule that minimizes $\mathbb{E}[c]$ is given by the likelihood ratio test [Duda et al. 2001]: $\frac{p(Y|H_1)}{p(Y|H_0)} \underset{\widetilde{H}_0}{\overset{\widetilde{H}_1}{\gtrless}} \frac{\mathbb{P}(H_0)}{\mathbb{P}(H_1)} \cdot \frac{C_{10}-C_{00}}{C_{01}-C_{11}}$. We now derive the likelihoods $p(Y|H_0)$ and $p(Y|H_1)$. When the target is present, $Y|H_0 = \sum_{i=1}^{N} n_i \sim \mathcal{N}\left(\mu, \sigma^2\right)$. When the target is present, $Y|H_1 = \sum_{i=1}^{N} s_i + \sum_{i=1}^{N} n_i \sim \mathcal{N}\left(\mu+S, \sigma^2\right)$. Hence, $p(Y|H_0) = \phi(Y|\mu, \sigma^2)$ and $p(Y|H_1) = \phi(Y|\mu + S, \sigma^2)$, where $\phi(x|\mu, \sigma^2)$ is the probability density function of the normal distribution $\mathcal{N}(\mu, \sigma^2)$, i.e., $\phi(x|\mu, \sigma^2) = \frac{1}{\sqrt{2\pi}\sigma} \exp\left(-\frac{(x-\mu)^2}{2\sigma^2}\right)$. Therefore, the likelihood ratio is $\frac{p(Y|H_1)}{p(Y|H_0)} = \exp\left(\frac{(2Y-2\mu-S)S}{2\sigma^2}\right)$ and the likelihood ratio test becomes the threshold-base decision rule presented in Section 4.2.

B. ERROR ANALYSIS FOR FEEDBACK OF HIGH-QUALITY SENSOR

As the high-quality sensor can detect the target with high fidelity, the number of false alarms and misses made by the low-end sensors (i.e., n_{f1} and n_{d1}, respectively) can be accurately estimated. Therefore, we ignore the detection errors of the high-quality sensor in the following analysis. The true P_{FL} is given by $P_{FL} = \frac{n_{f1}}{n_0}$, where n_0 denotes the number of detections when no target is present. As the estimate $\widetilde{P}_{FL}$ given by (5) uses the mean value of n_0, i.e., $\widetilde{P}_{FL} = \frac{n_{f1}}{\mathbb{E}[n_0]}$ where $\mathbb{E}[n_0] = m - m \cdot P_a$, the error of $\widetilde{P}_{FL}$ is mainly due to the fluctuation of n_0. The relative error of $\widetilde{P}_{FL}$, denoted by e, is given by $e = \frac{\widetilde{P}_{FL}-P_{FL}}{P_{FL}} = \frac{n_0-\mathbb{E}[n_0]}{\mathbb{E}[n_0]}$. Moreover, $\mathrm{Var}[n_0] = \mathbb{E}[(n_0 - \mathbb{E}[n_0])^2] = \mathbb{E}[e^2(\mathbb{E}[n_0])^2] = \mathbb{E}[e^2](\mathbb{E}[n_0])^2$, where $n_0 - \mathbb{E}[n_0]$ is replaced by $e\mathbb{E}[n_0]$. Therefore, the relative root mean square error (RRMSE) [NIST/SEMATECH 2010] of $\widetilde{P}_{FL}$ is given by $\mathrm{RRMSE} = \sqrt{\mathbb{E}[e^2]} = \frac{\sqrt{\mathrm{Var}[n_0]}}{\mathbb{E}[n_0]} = \sqrt{\frac{P_a}{1-P_a} \cdot \frac{1}{m}}$. Note that as n_0 follows the binomial distribution with success probability of $1 - P_a$, $\mathrm{Var}[n_0] = m(1 - P_a)P_a$. The error analysis for $\widetilde{P}_{ML}$ is omitted as it has similar result. Suppose the accuracy requirement is $\mathrm{RRMSE} \leq \epsilon$, we can choose $m \geq \frac{P_a}{1-P_a} \cdot \frac{1}{\epsilon^2}$. For instance, if $P_a = 10\%$, we can choose $m = 50$ to achieve an accuracy of $\epsilon = 5\%$.

C. STABILITY ANALYSIS ON FEEDBACK DELAY

In this section, we discuss the impact of feedback delay on the calibration algorithm in Section 6. When $H(z) = z^{-d}$, the closed-loop transfer function of the system is $T_c(z) =$

$\frac{G_c(z)G_p(z)}{1+G_c(z)G_p(z)H(z)} = \frac{\frac{2aS}{\sigma^2}\cdot z^d}{z^d - z^{d-1} + \frac{2aS}{\sigma^2}}$. Note that $G_c(z) = \frac{a}{1-z^{-1}}$ which is derived in Section 6. The characteristic polynomial is $P(z) = z^d - z^{d-1} + \frac{2aS}{\sigma^2}$. In the Jury test [Ogata 1995], the following conditions must be satisfied for the system stability under any $d > 1$: 1) $\left|\frac{2aS}{\sigma^2}\right| > 1$; 2) $P(1) > 0$; and 3) $(-1)^d \cdot P(-1) > 0$. By solving the above inequalities, we have $\frac{\sigma^2}{2S} < a < \frac{\sigma^2}{S}$. We now investigate the stability condition under particular d. From the Jury stability tables shown in Fig. 14, the stability condition for $d = 2$ is $\left|\frac{2aS}{\sigma^2}\right| > 1 \bigcap \frac{\sigma^2}{2S} < a < \frac{\sigma^2}{S}$, i.e., $\frac{\sigma^2}{2S} < a < \frac{\sigma^2}{S}$, and the stability condition for $d = 3$ is $\left|\left(\frac{2aS}{\sigma^2}\right)^2 - 1\right| > \left|-\frac{2aS}{\sigma^2}\right| \bigcap \frac{\sigma^2}{2S} < a < \frac{\sigma^2}{S}$, i.e., $\frac{1+\sqrt{5}}{4}\cdot\frac{\sigma^2}{S} < a < \frac{\sigma^2}{S}$. The stability conditions for $d = 4$ and $d = 5$ are $0.901\cdot\frac{\sigma^2}{S} < a < \frac{\sigma^2}{S}$ and $0.94\cdot\frac{\sigma^2}{S} < a < \frac{\sigma^2}{S}$, respectively, which are computed via numerical method.

D. EVALUATION OF MONOTONICITY

In this section, we evaluate the monotonicity of $f(\boldsymbol{\alpha}, \boldsymbol{\beta})$ with respect to $\sum_{i=1}^{N}(\alpha_i + \beta_i)$ by Monte Carlo method. For each trial, two points are randomly and uniformly sampled from the $2N$-dimensional space $\{\alpha_i, \beta_i | i \in [1, N], \alpha_i \in (0, 1), \beta_i \in (0, 1)\}$ to calculate $f(\boldsymbol{\alpha}, \boldsymbol{\beta})$ and $\sum_{i=1}^{N}(\alpha_i + \beta_i)$. We conduct a large number of trials (10^6 in this paper) to estimate the probability that $f(\boldsymbol{\alpha}, \boldsymbol{\beta})$ decreases with $\sum_{i=1}^{N}(\alpha_i + \beta_i)$. Fig. 15 plots the probability that $f(\boldsymbol{\alpha}, \boldsymbol{\beta})$ decreases with $\sum_{i=1}^{N}(\alpha_i + \beta_i)$ versus the number of sensors, i.e., N. The results show that $f(\boldsymbol{\alpha}, \boldsymbol{\beta})$ decreases with $\sum_{i=1}^{N}(\alpha_i + \beta_i)$ with a high probability ($> 98\%$ when $N \geq 3$).

REFERENCES

ADBELZAHER, T., DIAO, Y., HELLERSTEIN, J. L., LU, C., AND ZHU, X. 2008. *Performance Modeling and Engineering*. Springer, Chapter Introduction to Control Theory and its Application to Computing Systems, 185–215. SIGMETRICS'08.

ASH, R. B. AND DOLÉANS-DADE, C. A. 1999. *Probability & Measure Theory* 2nd Ed. A Harcourt Science and Technology Company.

BALZANO, L. AND NOWAK, R. 2007. Blind calibration of sensor networks. In *IPSN*. ACM.

BYCHKOVSKY, V., MEGERIAN, S., ESTRIN, D., AND POTKONJAK, M. 2003. A collaborative approach to in-place sensor calibration. In *IPSN*. ACM.

CHAIR, Z. AND VARSHNEY, P. 1986. Optimal data fusion in multiple sensor detection systems. *IEEE Trans. Aerospace Electron. Syst. 22,* 1, 98–101.

CHEN, J., TAN, R., XING, G., WANG, X., AND FU, X. 2010. Fidelity-aware utilization control for cyber-physical surveillance systems. In *RTSS*. IEEE.

CLOUQUEUR, T., SALUJA, K. K., AND RAMANATHAN, P. 2004. Fault tolerance in collaborative sensor networks for target detection. *IEEE Trans. Comput. 53,* 3, 320–333.

DUARTE, M. AND HU, Y.-H. 2003. Distance based decision fusion in a distributed wireless sensor network. In *IPSN*. ACM.

DUARTE, M. AND HU, Y.-H. 2004. Vehicle classification in distributed sensor networks. *J. Parallel and Distributed Computing 64,* 7, 826–838.

DUDA, R., HART, P., AND STORK, D. 2001. *Pattern Classification*. Wiley.

DUTTA, P., ARORA, A., AND BIBYK, S. 2006. Towards radar-enabled sensor networks. In *IPSN*. ACM.

DUTTA, P., GRIMMER, M., ARORA, A., BIBYK, S., AND CULLER, D. 2005. Design of a wireless sensor network platform for detecting rare, random, and ephemeral events. In *IPSN*. ACM.

FENG, J., MEGERIAN, S., AND POTKONJAK, M. 2003. Model-based calibration for sensor networks. In *Sensors*. IEEE.

GIROD, L., LUKAC, M., TRIFA, V., AND ESTRIN, D. 2006. The design and implementation of a self-calibrating distributed acoustic sensing platform. In *SenSys*. ACM.

HATA, M. 1980. Empirical formula for propagation loss in land mobile radio services. *IEEE Trans. Veh. Technol. 29,* 3, 317–325.

HE, T., KRISHNAMURTHY, S., STANKOVIC, J. A., ABDELZAHER, T., LUO, L., STOLERU, R., YAN, T., GU, L., HUI, J., AND KROGH, B. 2004. Energy-efficient surveillance system using wireless sensor networks. In *MobiSys*. ACM.

HWANG, J., HE, T., AND KIM, Y. 2007. Exploring in-situ sensing irregularity in wireless sensor networks. In *SenSys*. ACM.

IHLER, A., FISHER III, J., MOSES, R., AND WILLSKY, A. 2004. Nonparametric belief propagation for self-calibration in sensor networks. In *IPSN*. ACM.

KIM, Y., SCHMID, T., CHARBIWALA, Z. M., FRIEDMAN, J., AND SRIVASTAVA, M. B. 2008. NAWMS: Nonintrusive autonomous water monitoring system. In *SenSys*. ACM.

KIM, Y., SCHMID, T., CHARBIWALA, Z. M., AND SRIVASTAVA, M. B. 2009. ViridiScope: design and implementation of a fine grained power monitoring system for homes. In *Ubicomp*. ACM.

LE, H., HENRIKSSON, D., AND ABDELZAHER, T. 2007. A control theory approach to throughput optimization in multi-channel collection sensor networks. In *IPSN*. ACM.

LI, D. AND HU, Y.-H. 2003. Energy based collaborative source localization using acoustic micro-sensor array. *J. EUROSIP Applied Signal Processing 2003,* 4, 321–337.

MOTEIV CORP. 2006. Tmote sky datasheet. `http://www.moteiv.com/`.

NIST/SEMATECH. 2010. *e-Handbook of Statistical Methods*. National Institute of Standards and Technology. `http://www.itl.nist.gov/div898/handbook/`.

NIU, R. AND VARSHNEY, P. K. 2005. Distributed detection and fusion in a large wireless sensor network of random size. *J. EURASIP Wireless Communications and Networking 2005,* 4, 462–472.

OGATA, K. 1995. *Discrete-time control systems*. Prentice-Hall.

RAMANATHAN, N., BALZANO, L., BURT, M., ESTRIN, D., HARMON, T., HARVEY, C., JAY, J., KOHLER, E., ROTHENBERG, S., AND SRIVASTAVA, M. 2006. Rapid deployment with confidence: Calibration and fault detection in environmental sensor networks. Tech. rep., Center for Embedded Networked Sensing.

SHENG, X. AND HU, Y.-H. 2005. Maximum likelihood multiple-source localization using acoustic energy measurements with wireless sensor networks. *IEEE Trans. Signal Process. 53,* 1, 44–53.

SHI, L., JOHANSSON, K., AND MURRAY, R. 2007. Change sensor topology when needed: How to efficiently use system resources in control and estimation over wireless networks. In *CDC*. IEEE.

TAN, R., XING, G., LIU, B., AND WANG, J. 2009. Impact of data fusion on real-time detection in sensor networks. In *RTSS*. IEEE.

TAN, R., XING, G., WANG, J., AND SO, H. C. 2008. Collaborative target detection in wireless sensor networks with reactive mobility. In *IWQoS*. IEEE.

TAN, R., XING, G., WANG, J., AND SO, H. C. 2010. Exploiting reactive mobility for collaborative target detection in wireless sensor networks. *IEEE Trans. Mobile Comput.*. To appear in the March issue, 2010.

VARSHNEY, P. K. 1996. *Distributed Detection and Data Fusion*. Springer.

VIGORITO, C., GANESAN, D., AND BARTO, A. 2007. Adaptive control of duty cycling in energy-harvesting wireless sensor networks. In *SECON*. IEEE.

WHITEHOUSE, K. AND CULLER, D. 2002. Calibration as parameter estimation in sensor networks. In *WSNA*. ACM.

WOO, A., TONG, T., AND CULLER, D. 2003. Taming the underlying challenges of reliable multihop routing in sensor networks. In *SenSys*. ACM.

WREN, C., ERDEM, U., AND AZARBAYEJANI, A. 2006. Functional calibration for pan-tilt-zoom cameras in hybrid sensor networks. *Multimedia Systems 12,* 3, 255–268.

XING, G., TAN, R., LIU, B., WANG, J., JIA, X., AND YI, C.-W. 2009. Data fusion improves the coverage of wireless sensor networks. In *MobiCom*. ACM.

ZUNIGA, M. AND KRISHNAMACHARI, B. 2004. Analyzing the transitional region in low power wireless links. In *SECON*. IEEE.

Received February 2010; revised August 2010; accepted December 2010